Engine air intake design and evaluation - examples from the Bluecopter™ demonstrator

A. Garavello, T. Kneisch, M. Müller, A. D'Alascio
Airbus Helicopters Deutschland GmbH
Industriestraße 4, 86609 Donauwörth, Germany

Abstract

The Bluecopter demonstrator was developed to prove the feasibility of future eco-friendly rotorcraft by demonstrating significant reduction of CO_2 emission, fuel consumption and noise (Ref. 1). In this context, several different engine air intake configurations were designed and tested, with the aim of improving engine efficiency and reducing fuel consumption, with minimal to no impact on airframe drag. The present paper summarizes the engine intake design, optimization and testing activities carried out in the frame of the Bluecopter project.

1. NOTATION

Symbols

C_2	Pressure jump coefficient, [-]
d	Porous medium thickness, [m]
DC_{60}	Total pressure distortion, [-]
$DC_{60,\mathrm{NORM}}$	Normalized DC_{60}, [-]
$DC_{60,\mathrm{REF}}$	Reference DC_{60}, [-]
GM	Gross mass, [kg]
IAS	Indicated Air Speed, [kt]
IG	Generator current, [A]
MGT	Measured gas temperature, [°C]
MGT_c	Corrected MGT, [°C]
NG	Gas generator speed, [rpm, %]
NG_c	Corrected NG, [rpm, %]
NPT	Free turbine speed, [rpm, %]
OAT	Outside Air Temperature, [°C]
$PAMB$	Ambient Pressure, [Pa]
P	Static pressure, [Pa]
P_t	Total pressure, [Pa]
$P_{t,\infty}$	Free stream P_t, [Pa]
$\bar{P}_t$	Average P_t, [Pa]
$\bar{P}_{t,AIP}$	AIP $\bar{P}_t$, [Pa]
$\bar{P}_{t,FOD}$	FOD grid $\bar{P}_t$, [Pa]
$\bar{P}_{t,low}$	Lowest $\bar{P}_t$ over 60° AIP secor, [Pa]
$PWSD$	Engine power, [kW]
$PWSD_c$	Corrected PWSD, [kW]
$PWSD_{uninst}$	Uninstalled engine power, [kW]
$P3$	Engine Compressor discharge pressure, [bar]
ROC	Rate of climb, [ft/min]
TRQ	Engine torque, [Nm, %]
TAS	True Air Speed, [kt]
U	Air speed, [m/s]
U_∞	Free stream speed, [m/s]
$U_{\infty,max}$	Maximum free stream speed, [m/s]
UG	Generator voltage, [V]
WF	Fuel consumption, per engine [kg/h]
WF_{uninst}	Uninstalled WF, [kg/h]
WF_c	Corrected WF, [kg/h]
XF	δ exponent for WF correction, [-]
XN	δ exponent for NG correction, [-]
XP	δ exponent for PWSD correction, [-]
XT	δ exponent for MGT correction, [-]
YF	θ exponent for WF correction, [-]
YN	θ exponent for NG correction, [-]
YP	θ exponent for PWSD correction, [-]
YT	θ exponent for MGT correction, [-]
α	Porous medium permeability, [-]
δ	Corrected pressure, [-]
η	Total pressure ratio, [-]
η_{NORM}	Normalized η, [-]
η_{REF}	Reference η, [-]
$\eta_{NORM,AIP}$	η_{NORM} on AIP, [-]
$\eta_{NORM,FOD}$	η_{NORM} on FOD grid, [-]
θ	Corrected temperature, [-]
μ	Air dynamic viscosity, [sPa]
ρ	Air density, [kg/m^3]

Acronyms:

AHD	Airbus Helicopters Deutschland
AIP	Aerodynamic Interface Plane
BSL	Baseline (intake configuration)

CAD	Computer Aided Design
CFD	Computational Fluid Dynamic
EEPP	Estimated Engine Performance Program
GRC	Green Rotorcraft Consortium
FOD	Foreign Object Damage
IBF	Inlet Barrier Filter
ISA	International Standard Atmosphere
MCP	Maximum Continuous Power
OEI	One Engine Inoperative
PWC	Pratt & Whitney Canada
SL	Sea Level
TOP	Take-Off Power
TUM-AER	Technical University of Munich, Aerodynamic institute

2. INTRODUCTION

The Airbus Bluecopter (Figure 1) was a technology demonstrator derived from the H135 twin engine helicopter and developed in the context of several German research projects (LuFo) and the Clean Sky initiative. Several novel technologies were studied and tested on the Bluecopter demonstrator, including:

- Two new bearingless five-bladed main rotors, namely IKOROZ (with BlueEdge™ blade design, Ref. 1) and GRC1 (Ref. 2);
- Improved airframe aerodynamics with full-faired rotor head, faired landing skids and backdoor strakes (Ref. 3);
- T-Tail horizontal stabilizer, featuring an active fin rudder (Ref. 4);
- New Fenestron design, including acoustic liner technology;
- Acoustic rotor speed laws;
- "Eco-mode" power management (based on intended single engine operations) and more.

The Bluecopter was successfully flight tested between 2014 and 2016, demonstrating significant improvements with respect to the reference rotorcraft in terms of noise (Ref. 4), flight performance and fuel consumption (Ref. 1), while, at same time, mastering the aeromechanic challenges introduced by the eco-friendly design (Ref. 5). The GRC1 five-bladed main rotor, now equipping the latest version of the H145 (BK117 D-3), is a successful example of transferring technology from a research demonstrator into a serial product.

Within the scope of the Bluecopter demonstrator, new engine air intake designs were developed, analyzed and tested with the goal of reducing power losses and fuel consumption due to installation effects with respect to the baseline H135 configuration. The air intake design cycle consisted of three main steps:

- Layout of several engine air intake variants and their evaluation through Computational Fluid Dynamics (CFD);
- Wind tunnel tests, carried out in the framework of the Clean Sky partner project ATHENAI at the Technical University of Munich, aerodynamics institute (Ref. 6, 7, 8, 9, 10);
- Final flight test evaluation of three down selected intake variants on the Bluecopter demonstrator.

The following chapters outline the main results achieved during the three development steps, highlight the accuracy of numerical predictions against measurements in wind tunnel and flight tests, and finally summarize the possible gains against the reference configuration.

The design of an effective and functioning air induction system for a helicopter turboshaft engine is a complex engineering task, involving trade studies between several disciplines in addition to aerodynamics and engine performance, such as overall helicopter architecture, weight impact, environmental protection (ice accretion, snow ingestion, hot gases recirculation etc.), noise and others. This paper however focuses on the aerodynamics and performance aspects only.

Figure 1: The Bluecopter™ demonstrator.

3. AIR INTAKE DESIGN

3.1. Baseline configuration (Static Intake)

Two Pratt & Whitney Canada (PWC) PW206B turboshaft engines powered the Bluecopter demonstrator. This small turboshaft, featuring a radial inlet feeding a single stage centrifugal compressor (Figure 2), already equipped the serial H135 helicopter. It was therefore a natural choice to take the H135 static air intake (Figure 3) as reference configuration on which to base the Bluecopter demonstrator air intake optimization studies.

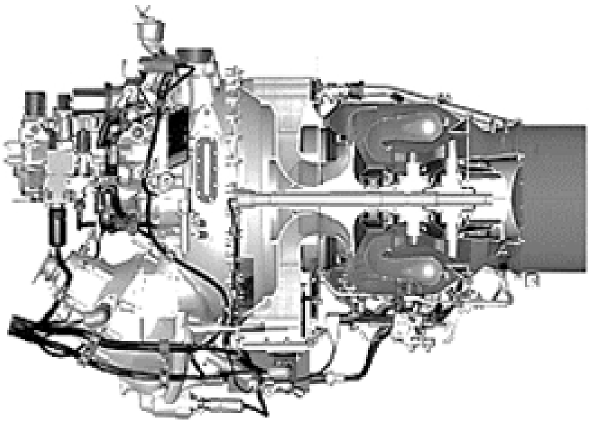

Figure 2: PW206B cross section (Ref. 11).

Figure 3: H135 static air intake serial design.

The outer shape of the static intake geometry was subject of design investigations aiming at improving the overall aerodynamic efficiency, although, due to structural reasons, only part of the engine cowling could be modified. Some additional constraints like the mast fairing, the engine fixed fire walls and an existing NACA inlet, employed for the ventilation of the engine compartment, had to be considered.

The air entering the static air intake is fed to the radial engine inlet through a plenum chamber. The reference design is based on the serial H135 plenum (Figure 4), which in turns derives from the former EC135 configuration: this helicopter is equipped with a dynamic air intake leading the air through the upper deck and entering the plenum from the inside. The most recent H135 switched to a static air intake, feeding the plenum from the outside, but retaining the original design as bypass when the engine inlet filtration system (IBF) is installed. Due to the research nature of the project, the shape of the engine plenum could be changed sensibly in order to investigate the effect on aerodynamic efficiency and engine performance.

On the serial H135 an additional FOD grid is mounted in front of the engine opening (Figure 5) in order to protect the installed engines from damage and icing. This design feature has been taken over for the Bluecopter and modified to fit the different intake variants which were developed. The engine itself is delivered with its own FOD grid installed around the radial compressor inlet.

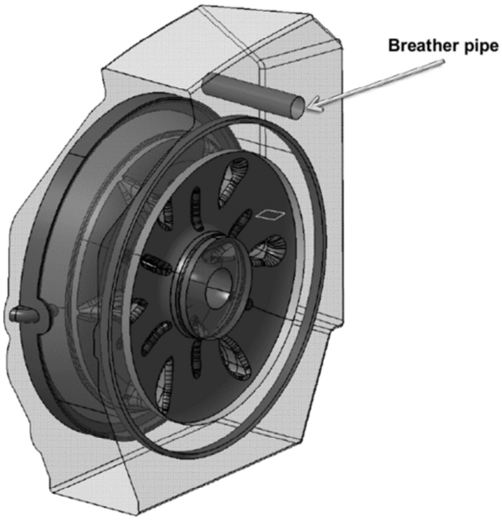

Figure 4: Baseline plenum design (CAD left engine).

Figure 5: Baseline FOD grid as installed on the H135.

3.2. Design variants and optimization

Starting from the reference air intake described in the previous chapter, several optimization loops have been carried out involving the static intake outer shape, the plenum shape and the FOD grid. The aim of the optimization studies was to improve the overall aerodynamic efficiency of the engine installation, so as to reduce fuel consumption, in line with the Bluecopter project high level objectives.

The Bluecopter new air intake development was carried out in two steps:

1. the cowling and plenum chamber were modified, targeting for a balanced design well compromising performance in both hover and level flight;
2. several add-ons were then investigated aiming specifically at improving performance in level flight,

During step one, the trade studies evaluated six different intake outer shapes, four plenum chamber designs and two FOD grids. Modifications of the outer cowling shape mainly focused in pushing the cowling surface upstream of the engine inlet inboard, so as to create a "ramp" intended for improving the pressure recovery in forward flight (*Figure 6*). The ramp intake was investigated in six different variants, analyzing the effect of the ramp depth into the cowling, smoothed corners and of a boundary layer separator placed on the ramp surface.

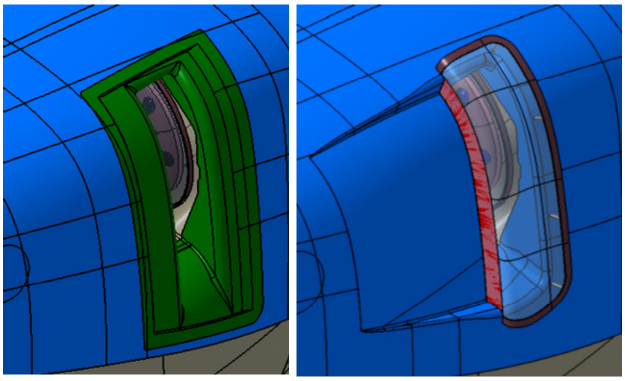

(a) (b)

Figure 6: Baseline static intake (a) compared to the ramp intake with modified FOD grid (b).

On the plenum side, efforts were concentrated in rounding the plenum walls (*Figure 7*- a) with respect to the baseline design (Figure 4). Additional aerodynamic features have been subsequently investigated, targeting a more uniform flow distribution between the inner and outer part of the plenum. Such solutions included a flow deflector (*Figure 7*– b) and a guide vane in the lower-inner part of the plenum.

As previously mentioned, a second set of modifications were investigated in order to study add-on solutions, to be mounted on top of the configuration finalized during step one, dedicated to further improve performance in forward flight. One such add-on is the scoop intake (*Figure 8*). Several scoop intake versions have been analyzed, varying its front opening surface, lip radius and detailed lofting onto the engine cowling.

Other add-ons, which were considered during the design phase, were an inlet guide-vane (*Figure 9*) and a rear spoiler (*Figure 10*). Both designs, were directly tested in the wind tunnel (Ref. 8) with no previous aerodynamic analysis carried out at AHD.

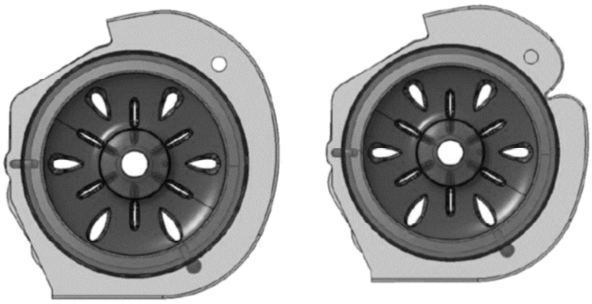

(a) (b)

Figure 7: Modified inlet plenum chamber with rounded shape (a) and with additional flow deflector (b).

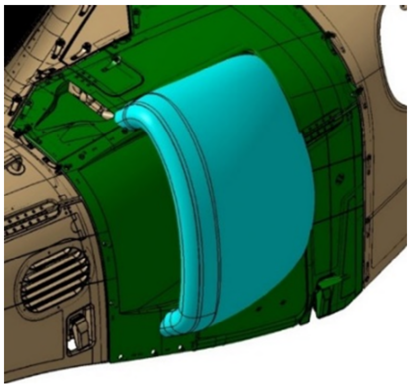

Figure 8: Scoop intake, mounted on top of the ramp-intake as add-on.

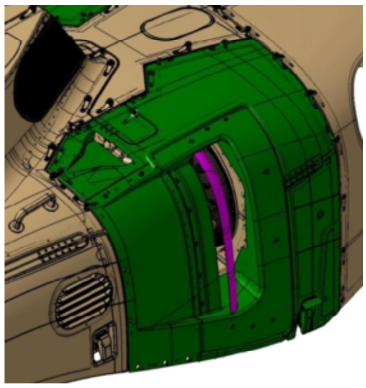

Figure 9: Inlet guide vane, mounted on the ramp-intake as add-on.

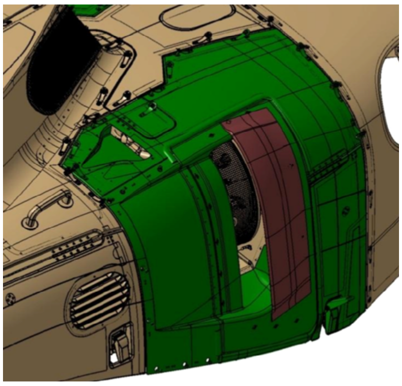

Figure 10: Rear spoiler, mounted on top of the ramp-intake as add-on.

3.3. Analysis methods

The aerodynamic analysis of the several intake variants has been initially carried out by means of numerical simulation previous to wind tunnel testing (see chapter 4). Computational Fluid Dynamics (CFD) simulations were carried out by means of the unstructured Unsteady Reynolds Averaged Navier-Stokes (URANS) code FLUENT 14.5 on unstructured meshes generated with the commercial grid generator ICEM CFD, both distributed by ANSYS. Computations were carried out in steady state mode, applying the k-ε turbulence model with enhanced wall functions.

The original CAD model of the Bluecopter fuselage was simplified by removing part of the tail boom, empennage and the landing skids to reduce the meshing workload and the computational time. Furthermore, the geometry was cleaned from screws, holes, washers and any other features deemed irrelevant for the aerodynamic analysis of interest. *Figure 11* shows the part setup of the CFD model employed for the aerodynamic analysis. Aerodynamic loads and moments could be computed separately on each of the components and then added up in post-processing. All parts were furthermore divided into left and right hand side of the helicopter. The surface “AIP” (*Figure 11*- b) represents the entry to the engine compressor, where the needed mass flow is taken out of the computational domain by means of a mass flow rate boundary condition. The same mass flow (slightly increased by the engine fuel flow) is released back into the computational domain through exhaust surfaces.

The effect of the helicopter main rotor on the flow field affecting the air intake was modelled by means of a volumetric actuator disc; the actuator disc model reproduces the rotor downwash and swirl by applying a prescribed load on the volumetric region defined by the rotor disc. The prescribed load was computed in hover and forward flight by means of a blade element theory model of the Bluecopter rotor, embedded within the Bluecopter flight dynamics model.

The outer FOD grid (*Figure 11*- c) and the inner engine grid are both modelled by means of an additional interior surface. The approach here was to apply a boundary condition available in FLUENT called “porous-jump” modelling a loss of total pressure as a function of the velocity normal to the porous surface, via a linear and a quadratic term, over the given surface, as given by equation (1) in Ref. 12.

$$\Delta P_t = -\left(\frac{\mu}{\alpha}U + C_2\frac{1}{2}\rho U^2\right)d \qquad (1)$$

With the model parameters permeability (α), porous medium thickness (d) and pressure jump coefficient (C_2) derived from Ref. 13.

All unstructured meshes were generated using the mesh generator ICEM CFD 14.5. To resolve the boundary layer, prism-layers were generated on all solid-surfaces of the model. The helicopter was placed in a far-field box with a size of 100m x 100m x 80m. The resulting total number of cells is 45 million. To save computational time and resources the boundary layer consisted of 10 prism-layers, therefore the application of the wall-function approach was necessary. *Figure 12* shows some details concerning the CFD model surfaces, the associated surface mesh and close-up view of the unstructured volume mesh.

All CFD computations have been carried out at the atmospheric/flight conditions reported in Table 1.

The engine mass flow rates imposed on the inlet/outlet boundary surfaces for the engine intake and exhaust were computed by means of the PW206B estimated engine performance program (EEPP) provided by PWC, at the given power required. The actuator disc (rotor) loads and the aircraft attitude angles have been determined by means of the Bluecopter flight dynamic model implemented within the AHD flight mechanics software GENSIM (Ref. 14). The same model was also utilized to determine the helicopter power required, input for the engine performance analysis and the determination of the inlet mass flow rate.

Following the CFD analysis, the integral pressure loss evaluated on the engine inlet plane (engine FOD grid) was input into the EEPP in order to comparatively evaluate power losses and fuel flow penalties. The available PW206B EEPP does not provide the capability to include flow distortion effects within the engine performance analysis. Therefore, total pressure distortion could not be accounted for in this step, although it may play a significant role (Ref. 15).

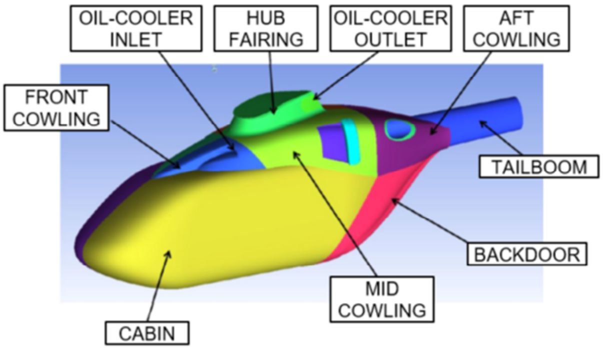

(a)

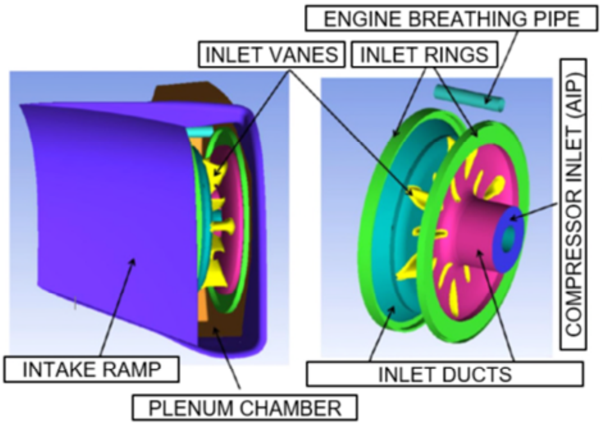

(b)

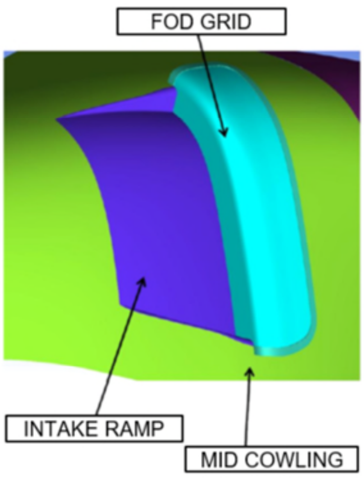

(c)

Figure 11: Part Setup for CFD computation: Fuselage (a), Intake (b) and FOD grid (c).

(a)

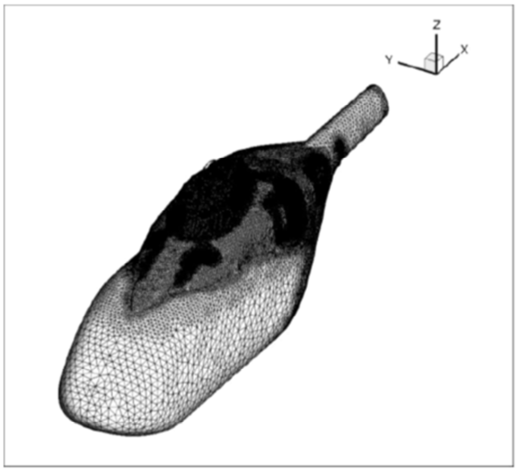

(b)

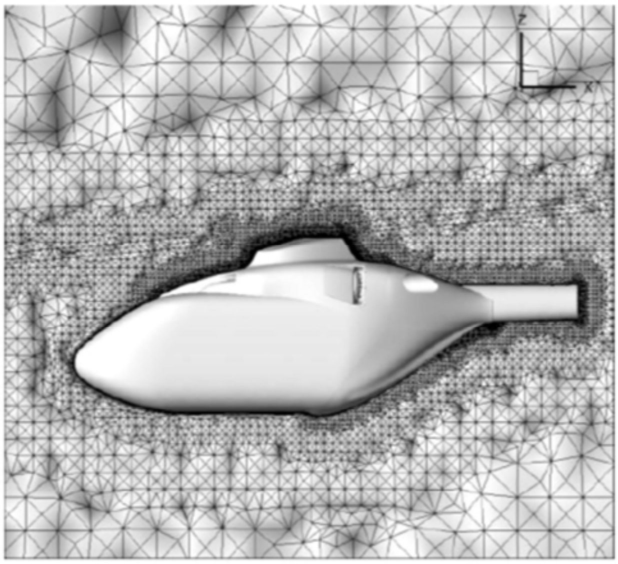

(c)

Figure 12: Surface geometry (a), the corresponding surface mesh (b) and close view to the unstructured volume mesh (c).

Table 1: Atmospheric and flight conditions considered for CFD analysis.

Characteristic	Hover	Level flight
Speed	0 kt	130 kt
Pressure	101325 Pa (SL)	
Density	1.14549 kg/m^3	
Temperature	308.15 K (ISA+20)	

3.4. Evaluation metrics

Several metrics have been employed to evaluate the aerodynamic characteristics and performance of the different air intake configurations analyzed:

- Inlet average total pressure ratio;
- Inlet total pressure distortion and swirl;
- Total configuration aerodynamic drag;
- Engine fuel flow reduction at constant power;
- Engine power available increase at MCP power rating;

As given in Ref. 6, for the investigation of the intake ram compression efficiency, a normalized total pressure ratio η_{NORM} is defined, equation (2). Within this paper, all total pressure ratios are normalized by the reference total pressure ratio, η_{REF}.

(2) $$\eta_{NORM} = \frac{\bar{P}_t}{P_{t,\infty}} \frac{1}{\eta_{REF}}$$

In equation (2), $P_{t,\infty}$ is the free stream total pressure, whereas $\bar{P}_t$ is the average total pressure on the inlet surface. Two different reference surfaces were employed for the η_{NORM} evaluation:

1. The AIP, $\eta_{NORM,AIP}$ as given by equation (3);
2. The engine FOD grid, $\eta_{NORM,FOD}$as given by equation (4).

The two provide similar trends and can be interchanged for the purpose of configuration ranking. However, the $\eta_{NORM,AIP}$ is more appropriate to evaluate the actual quality of the flow reaching the compressor, whereas $\eta_{NORM,FOD}$ is employed for the follow-up engine performance evaluation by means of the EEPP, which requires the total pressure at the engine FOD grid as input.

(3) $$\eta_{NORM,AIP} = \frac{\bar{P}_{t,AIP}}{P_{t,\infty}} \frac{1}{\eta_{REF}}$$

(4) $$\eta_{NORM,FOD} = \frac{\bar{P}_{t,FOD}}{P_{t,\infty}} \frac{1}{\eta_{REF}}$$

To evaluate the uniformity of the total pressure distribution on the AIP, the total pressure distortion coefficient $DC_{60,NORM}$ is applied (Ref. 16, normalized as in Ref. 6):

(5) $$DC_{60,NORM} = \frac{\bar{P}_{t,low} - \bar{P}_{t,AIP}}{\bar{q}_{AIP}} \frac{1}{DC_{60,REF}}$$

The DC_{60} gives the difference of the lowest average total pressure $\bar{P}_{t,low}$ segment with angular extent of 60° and the mean total pressure $\bar{P}_{t,AIP}$ in the AIP divided by the mean AIP dynamic pressure $\bar{q}_{AIP}$ (Ref. 7). Within this paper, all DC_{60} values are normalized by the reference total pressure distortion, $DC_{60,REF}$. The total pressure distortion level in the AIP is an indicator for stable engine operation (Ref. 17).

Another aspect considered in the global aerodynamic evaluation is the total fuselage drag variation. Indeed, even if an improved intake design was able to deliver higher pressure recovery to the engine, if this design increases the total aircraft drag, then the engine would have to run at a higher power level to compensate the increased power required of the helicopter to sustain the same flight condition in level flight. This effect could possibly nullify the benefits of the improved intake aerodynamic design.

Finally, the intake aerodynamic efficiency and total configuration drag information have been employed as input for the engine performance analysis. The inlet total pressure computed through CFD simulation (and related to $\eta_{NORM,FOD}$) can be input to the EEPP at a given power rating (MCP) in order to compute the difference in total power available delivered by the engine. The eventual power surplus can be used for instance to fly faster (in the regions of the flight envelope where power available is limited by the engine power). Within this paper, the power available variation is expressed as percentage difference with respect to the uninstalled engine power, according to equation (6).

(6) $$\Delta PWSD = \frac{PWSD - PWSD_{uninst}}{PWSD_{uninst}}$$

Where $PWSD$ is referred to the intake configuration under analysis. In case of total configuration drag change, then at MCP power the aircraft maximum speed changes accordingly (on the whole flight envelope, also in the regions where MCP power is limited by the MGB maximum torque rather than engine power).

Alternatively, the EEPP calculations can be carried out at constant input power, resulting in a change of fuel consumption. Within this paper, the fuel flow variation is expressed as percentage difference with respect to the uninstalled engine fuel flow, equation (7).

(7) $$\Delta WF = \frac{WF - WF_{uninst}}{WF_{uninst}}$$

Where WF is referred to the intake configuration under analysis. In case of total configuration drag change, then WF is computed at the actual power required of the new configuration.

3.5. Analysis results

For the sake of synthesis, analysis results are shown only for three air intake configurations, reflecting the geometries which were later tested in flight on the Bluecopter demonstrator:

- The static intake, H135 serial design (Figure 5 and *Figure 6*-a);
- The ramp intake (*Figure 6*-b);
- The scoop intake (scoop as add-on to ramp intake, *Figure 8*);

The detailed geometry of the ramp and scoop intakes considered here are the result of optimization studies looking at the best compromise between the aerodynamic and performance evaluation metrics listed in chapter 3.4. Both ramp and scoop intakes employ the modified (rounded) inlet plenum chamber with additional flow deflector (*Figure 7*-b).

Figure 13 and *Figure 14* show the normalized total pressure ratio computed at the FOD grid ($\eta_{NORM,FOD}$) and AIP ($\eta_{NORM,AIP}$) respectively. In the diagrams, bar groups indicate the two flight conditions considered (hover and level flight), whereas colors indicate different intake configuration data (static, ramp and scoop intake). In hover, the static and ramp intake are equivalent. The scoop intake shows a slight efficiency degradation of about 0.4%. In level flight, both the ramp intake and the scoop intake show improved efficiency with respect to the static intake: the ramp intake gains approximatively 1.5% efficiency (measured at the AIP) compared to the static. The scoop intake instead gains 2.4% against the static and approximatively 0.9% against the ramp intake.

The DC_{60} evolution is shown in *Figure 15*. The general trend, applicable to all three configurations, is for the DC_{60} to increase from hover to forward flight.

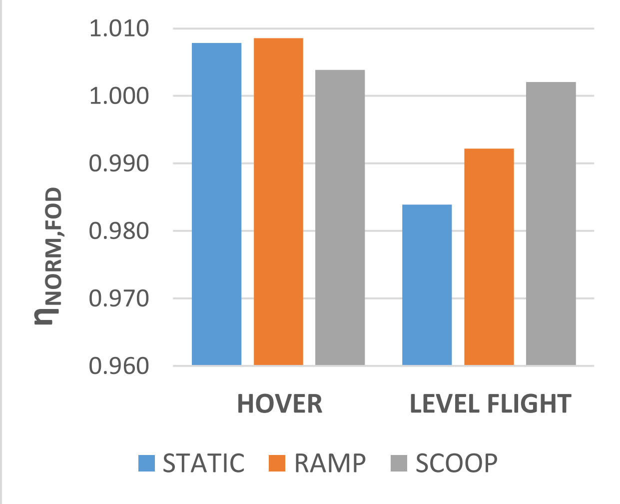

Figure 13: Normalized total pressure ratio measured at the engine FOD grid.

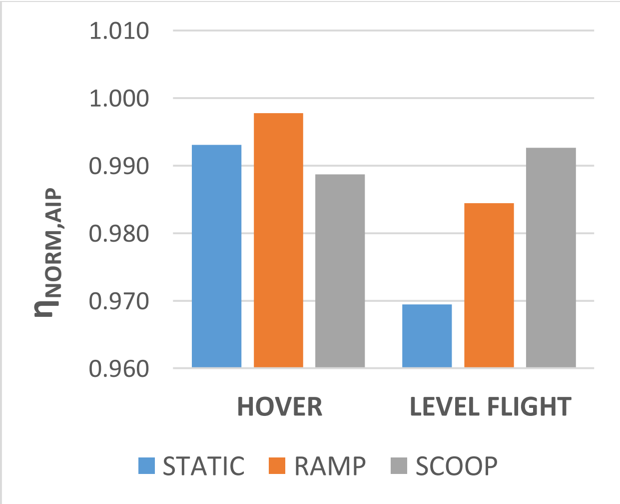

Figure 14: Normalized *total pressure ratio measured at the AIP (compressor inlet).*

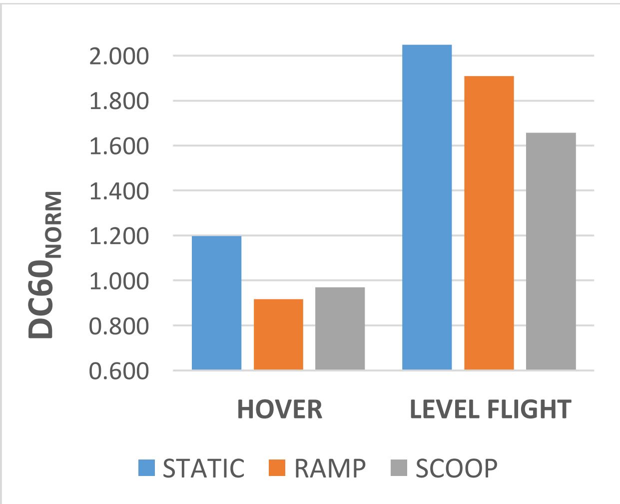

Figure 15: Normalized total pressure distortion (DC60) measured at the AIP (compressor inlet).

In hover, both ramp and scoop intake reduce DC_{60} by approximatively 20% with respect to the static intake. This effect is mostly attributed to the rounded plenum with additional flow deflector (*Figure 7*-b), as later confirmed by wind tunnel tests (Ref. 6, page 72). In level flight, the ramp design reduces the DC_{60} by 7% against the static one. The scoop intake instead, reduces DC_{60} by approximatively 20% with respect to the static intake and 13% against the ramp intake.

CFD simulations showed that the total contribution of the air intake to the total drag of the helicopter is rather small. When considering the simplified model as shown in *Figure 11*– a, approximatively 5 to 10% of total drag are contributed by the air intake (*Figure 16*). The relative contribution would be further reduced when considering the additional missing components, such as landing skids, rotor head and tail parts. With this introduction, the analysis of the airframe drag shows that the static and ramp intake have the same drag (as expected given the limited modification to the external geometry). The same conclusion holds for the scoop intake. However, given the more significant modification to the external shape, the analysis of the scoop intake drag is discussed in further details. Experimental investigations reported within Ref. 13 (chapter IX-2, Figure 14) show that the external drag coefficient due to a scoop intake for jet engine application should be zero when the intake is "matched" (i.e. the inlet mass flow from the incoming stream tube is equal to the mass flow required by the engine). This condition can be achieved by sizing the inlet capture area accordingly, using the design flight speed and engine mass flow rate as input parameter for the continuity equation. When the capture area is bigger than the "matched" one, the inlet opening is spilling and considerable parasite drag is caused by separation from the outside (Ref. 13). For helicopter applications however, adapting the capture area to cruise condition is unfavorable for hover flight, were instead large inlet surfaces are required. Guidelines for a compromise design choice resulting in only moderate drag increase are reported within Ref. 18. Specifically for the Bluecopter scoop intake, these design principles have been applied to choose the capture area so as to minimize the drag increase and at the same time provide a balanced intake performance in hover and level flight. The resulting geometry is analyzed in terms of drag and compared to the ramp intake in *Figure 17*: CFD simulations show that the scoop intake contribute to approximately 12% of the total airframe drag (on the simplified half model). This compares to the 6.5%, which is contributed by the ramp intake. Finally, the 5.5% points increase of intake drag was in absolute numbers very small and it was decided to neglect the scoop drag increase for the subsequent performance analysis.

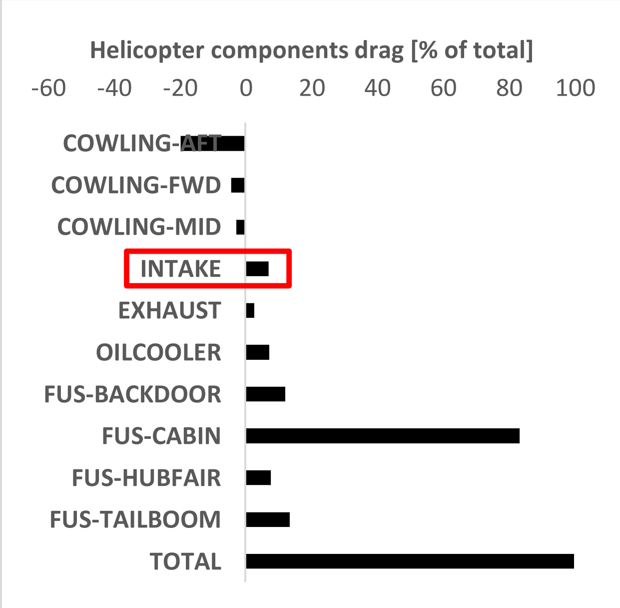

Figure 16: Fuselage drag breakdown (on simplified half model).

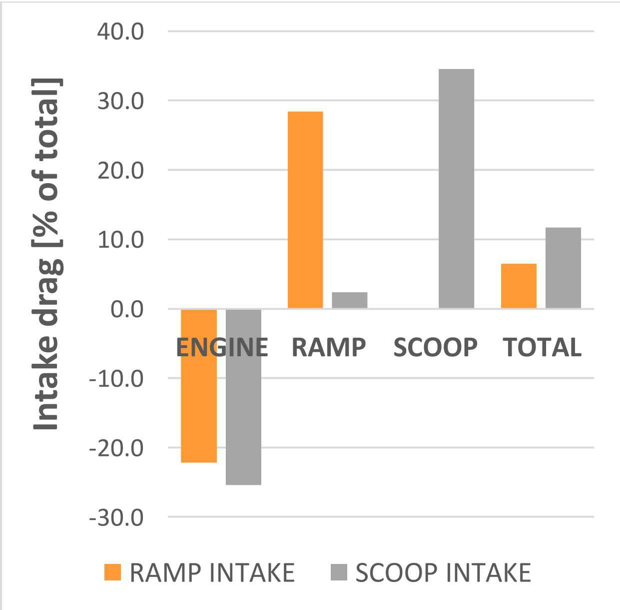

Figure 17: Intake variants drag comparison.

The results of the engine performance analysis carried out by means of the EEPP and exploiting the results discussed up to this point are reported in Table 2 and Table 3, respectively for the power available increase at MCP rating and fuel flow reduction at constant power. In terms of power available increase at MCP, in level flight, significant gains compared to the static configuration could be achieved: the ramp intake gains +2% power against the static, whereas the scoop gains +4% compared to static and + 2% against the ramp intake. In hover a slight degradation for the scoop intake has been calculated. Similar trends are observed for the fuel flow decrease at constant power (Table 3).

Table 2: Power available increase (at MCP rating) with respect to the static intake.

$\Delta PWSD - \Delta PWSD_{static}$	Hover	Level flight
Ramp Intake	0.00%	2.00%
Scoop Intake	-0.30%	4.00%

Table 3: Fuel consumption reduction with respect to the static intake.

$\Delta WF - \Delta WF_{static}$	Hover	Level flight
Ramp Intake	0.00%	-0.40%
Scoop Intake	0.25%	-1.00%

4. WIND TUNNEL TESTS

4.1. The project ATHENAI

The project ATHENAI (Aerodynamic Testing of Helicopter Novel Air Intakes) was launched in 2014 to support the Bluecopter demonstrator engine air intake development with wind tunnel tests. The institute of Aerodynamics and Fluid Mechanics at the Technical University of Munich (TUM-AER) carried out the experimental work, in collaboration with AHD. Results of the wind tunnel measurements are extensively documented in open literature (Ref. 6, 7, 8, 9 and 10). The following chapters provide an overview of the experimental activities as described in the aforementioned references and the main results, which are more relevant for the present paper.

4.2. Experimental setup

Experiments have been carried out at the wind tunnel facility A at TUM-AER, on a full-scale truncated fuselage section as shown in *Figure 18*. Flight conditions from hover to level flight were simulated in the wind tunnel open test section, up to maximum tunnel speed. The suction effect of the engine was instead simulated by means of a radial fan connected to the model AIP through a ducting system. *Figure 19* and Table 4 provide an overview of the wind tunnel setup as given in Ref. 7 and Ref. 8.

Extensive pressure measurements were recorded (see Ref. 7, chapter 5 for details on the measurement technique):

- On the AIP, total pressure and the three components of the velocity vector were acquired by means of four 5-holes probes mounted on a rake at four radial positions. The azimuthal total pressure distribution was fully covered by rotation of the rake;
- Static pressures were acquired at several locations on the outer cowling geometry, in the plenum chamber and on the inner engine inlet geometry leading to the AIP.

Many different intake configurations have been tested during the ATHENAI wind tunnel campaign: tests were structured around three baseline (BSL) configurations, namely the static (BSL1), ramp (BSL2) and scoop intake (BSL3), Ref. 7. *Figure 20* shows the three baseline wind tunnel models. BSL1 was combined with the serial plenum chamber as shown in Figure 4, whereas, initially, BSL2 and BSL3 were equipped with the rounded plenum geometry of *Figure 7*-a, Ref. 7. At a later stage, the additional flow deflector (*Figure 7*-b) was added to the wind tunnel models of BSL2 and BSL3 (Ref. 9), after investigating nine different azimuthal position and height combinations to identify the best deflector design.

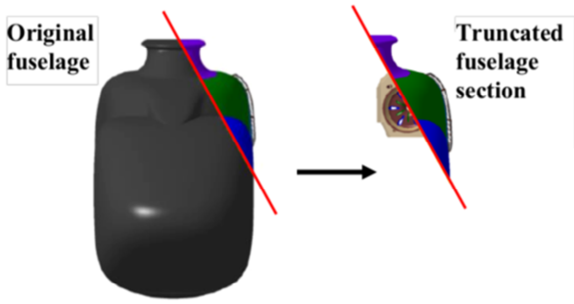

(a)

(b)

Figure 18: Truncation of the full-scale fuselage (a) (Ref. 8, fig. 2-a, page 3) and fuselage section model in the wind tunnel (b) (Ref. 8, fig. 3-a, page 4).

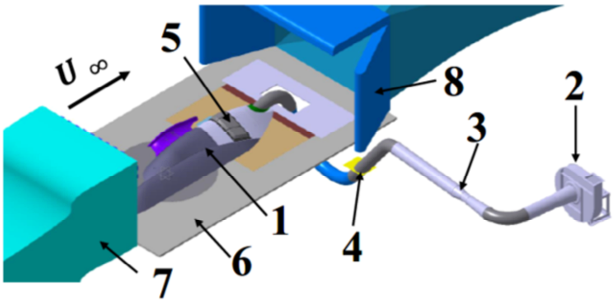

Figure 19: Overview of the wind tunnel setup (Ref. 8, figure 1, page 2).

Table 4: Components in the wind tunnel setup as shown in Figure 19 (from Ref. 8, table 1, page 3).

	Wind tunnel setup components
1	Fuselage section wind tunnel model
2	Radial fan
3	Venturi meter
4	Duct system
5	Air intake section
6	Wind tunnel floor
7	Wind tunnel nozzle
8	Wind tunnel collector

4.3. Main experimental results

Ref. 7 provides a detailed account of wind tunnel measurements focusing on the three initially defined baseline configurations. On the other hand, the results concerning the add-ons investigations are reported in Ref. 8. Ref. 9 provides a synthetized account for the three modified baseline intakes and the best retrofitted add-ons. The results from Ref. 9 are partially reported here, since they can be more readily compared against the numerical investigations in chapter 3.5 and the flight test results of chapter 5.4.

Figure 23 (from Ref. 9) shows the evolution of the normalized total pressure ratio against the free stream velocity (normalized by the maximum tunnel velocity). The modified baselines are here indicated as static (BSL1-mod), ramp (BSL2-mod) and scoop intake (BSL3-mod). It is worth mentioning that the prototype shop of AHD provided TUM-AER with the necessary FOD grids - for all intake configurations installed on the wind tunnel model - to make sure that the same level of pressure losses through the FOD grids is achieved in the wind tunnel as subsequently during flight tests. As discussed in Ref. 9, the ramp increases the ram effect with respect to the static intake, with an increased efficiency ($\eta_{NORM,AIP}$) of +0.5% almost constant at the higher speeds.

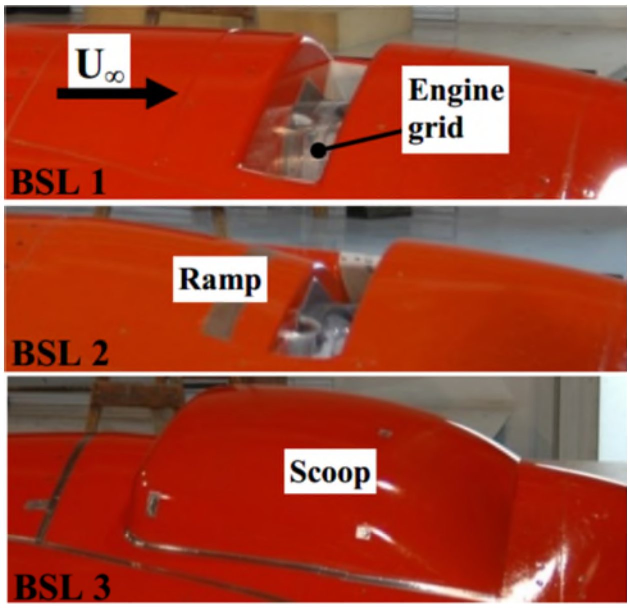

Figure 20: Baseline intake geometries tested in the wind tunnel (Ref. 9, fig. 7, page 4), static inlet (BSL1), ramp inlet (BSL2) and scoop inlet (BSL3).

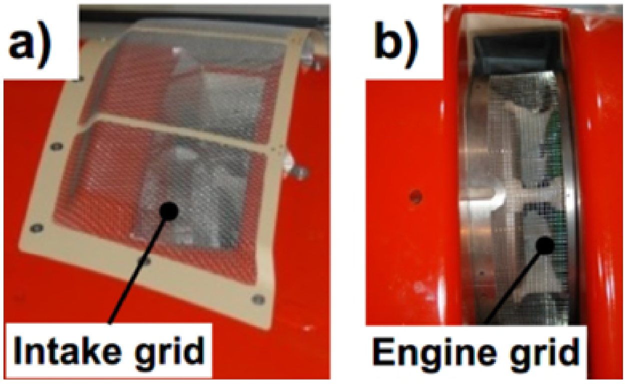

Figure 21: Intake (a) and engine (b) FOD grids on static intake model in the wind tunnel (Ref. 9, fig. 9, page 5). Each intake variant was equipped with an adapted FOD grid design.

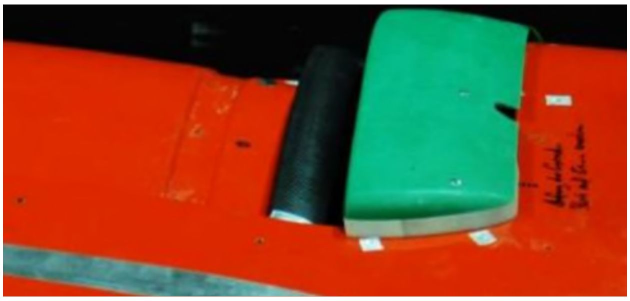

Figure 22: Example of retrofitted add-on on wind tunnel model: high/long rear spoiler with front inlet guide vane, mounted on ramp intake (BSL2-mod) (Ref. 8, fig. 6-b3, page 5).

Figure 23: Normalized total pressure ratio vs. freestream velocity for the three modified baseline and two best-retrofitted variants, at maximum corrected mass flow rate (Ref. 9, fig. 18, page 8).

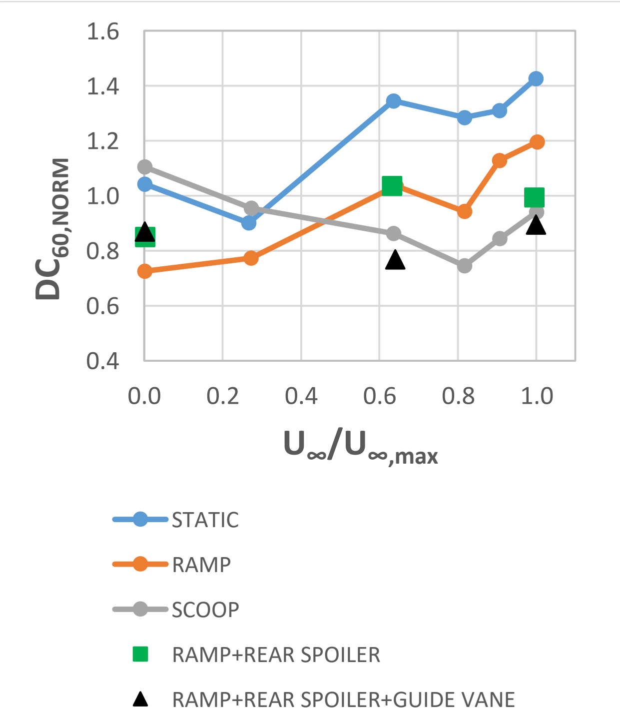

Figure 24: Normalized DC_{60} vs. freestream velocity for the three modified baseline and two best-retrofitted variants, at maximum corrected mass flow rate (Ref. 9, fig. 20, page 9).

The scoop intake further improves the ram effect with an additional +0.46% efficiency against the ramp intake. With respect to the static intake the scoop gains ~1% in ram compression efficiency as measured by $\eta_{NORM,AIP}$. Both best retrofit modifications show high level of total pressure at high speed, comparable with the scoop.

Figure 24 (from Ref. 9) shows the evolution of the normalized total pressure distortion coefficient against the free stream velocity (normalized by the maximum tunnel velocity). As discussed in Ref. 9, both the ramp and scoop intake improve the DC_{60} with respect to the static intake, with the ramp intake showing the lowest distortions. In level flight the DC_{60} increases for the static and ramp intake, whereas it globally decreases for the scoop intake. Both best retrofit modification show good DC_{60} levels in hover and level flight.

5. FLIGTH TESTS

5.1. Configurations tested in flight

Wind tunnel test results discussed in chapter 4.3 largely confirmed the trends highlighted by the numerical analysis reported in chapter 3.5. In light of these results, the ramp intake was chosen as engine air intake for the Bluecopter demonstrator, since it represents the best compromise between hover and level flight performance. In order to provide reference data, a first phase of tests was performed with the helicopter equipped with static (serial standard) intake. Finally, the scoop intake was chosen as add-on modification to be tested in a last phase of tests. Despite the promising results highlighted by wind tunnel tests on the best retrofit modifications (rear spoiler and guide vane), these solutions were not included in the flight test program due to time and budget constraints. *Figure 25* shows the three intake variants as assembled on the Bluecopter demonstrator.

The Bluecopter demonstrator had a dense and intensive test program, where many different technologies were evaluated. For this reason, it was not possible to test all three intake variants with a fully consistent helicopter configuration. In particular, the static intake flew in combination with the IKOROZ main rotor, the ramp intake in combination with both IKOROZ and the GRC1 main rotor, whereas the scoop intake flew only combined with the GRC1 rotor. The different rotor systems influence the engine performance characteristic due to their different rotor speed ranges, which in turn affects the engine turbomachines efficiency.

(a)

(b)

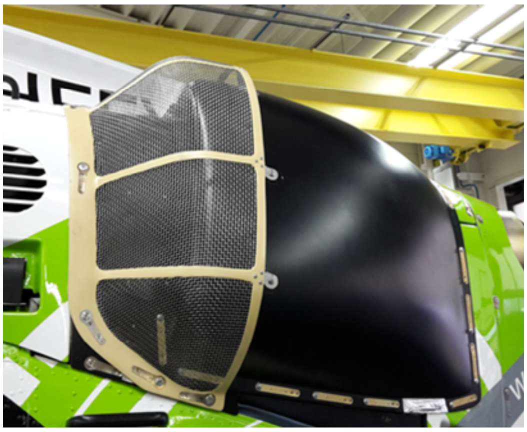

(c)

Figure 25: Air intake variants tested on the Bluecopter demonstrator: static (a), ramp (b) and scoop (c) intakes.

Table 5 summarizes the helicopter configurations tested in flight for the evaluation of the air intake performance. Flight test results for the ramp intake with the two different rotor systems were not perfectly consistent with each other due to the significant difference in rotor speed range, which cannot be easily accounted for with the normalization method employed to analyze the flight test data (chapter 5.3). Therefore, flight test results have been compared only between consistent helicopter configurations (Table 5): A vs. B (with IKOROZ rotor) and C vs. D (with GRC1 rotor). First, the relative performance of the ramp intake (B) is assessed against the static air intake (A), then, the scoop (D) intake is analyzed in relation to the ramp intake (C).

Table 5: Summary of configuration tested in flight for air intake performance evaluation.

	Intake	Main rotor	Rotor speed range (NPT)
A	STATIC	IKOROZ	80-90%
B	RAMP	IKOROZ	80-90%
C	RAMP	GRC1	90-100%
D	SCOOP	GRC1	90-100%

5.2. Flight test instrumentation

For the engine performance evaluation, the parameters recorded on the aircraft are summarized in Table 6. The engine parameters in Table 6 are recorded for both the left and right engine in order to enable the engine performance analysis on both sides.

Table 6: Summary of flight test parameters measured for evaluation of engine performance.

Name	Unit	Description
OAT	°C	Outside air temperature
PAMB	Pa	Ambient pressure
IAS	kt	Indicated air speed
ROC	ft/min	Rate of climb
NG	%	Engine gas generator speed
MGT	°C	Engine measured gas temperature
TRQ	%	Engine torque
NPT	%	Engine free turbine speed
WF	kg/h	Engine fuel flow
P3	bar	Compressor discharge pressure
IG	A	Generator current
UG	V	Generator voltage

The engine power, PWSD, is derived from the engine torque (TRQ) and the free turbine speed (NPT). The engine electrical generator load is derived from the generator current (IG) and voltage (UG). For all the flight test points considered in the frame of this analysis, the generator load was always kept at minimum (<1kW) and therefore neglected for the computation of power losses. The true air speed (TAS) is derived from the measured indicated air speed (IAS) by correcting for the air density effect and the calibration of the anemometry instruments. Finally, the engine fuel consumption (WF) was measured by means of a fuel mass flow meter.

Regrettably, it was not possible for AHD to access the internal parts of the engine inlet in order to properly instrument the AIP with total pressure sensors. Therefore, the measurement of the intake aerodynamic efficiency (in terms of total pressure ratio) and total pressure distortion in flight could not be carried out. Instead, both the ramp and plenum chamber were instrumented with static pressure probes as shown in *Figure 26*.

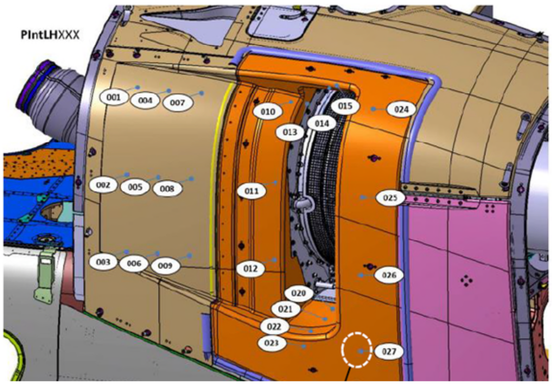

(a)

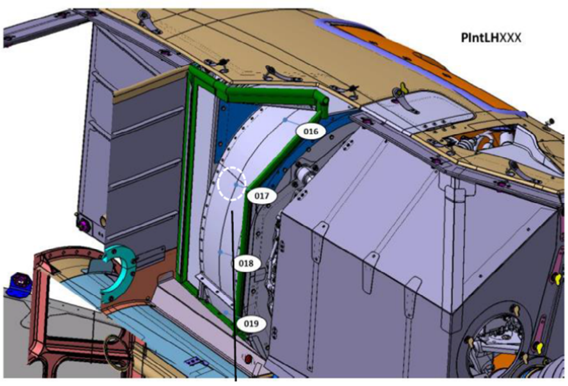

(b)

Figure 26: Pressure probes installed on the Bluecopter demonstrator air intake: on the ramp (a) and in the plenum chamber (b).

Inlet pressure instrumentation was available starting with configuration B (ramp intake) and on the left side engine only. No inlet pressure measurements have been carried out on the static air intake configuration.

In addition to pressure instrumentation, the engine inlet was instrumented with an array of thermocouples in order to monitor the average inlet temperature, temperature distortions and charge heating (*Figure 27*). The analysis of inlet temperatures is critical for flight conditions prone to exhaust gases re-ingestion (such as rearward flight). For the flight conditions considered here (hover and level flight) all intake variants behave similarly and therefore no inlet temperature analysis is included.

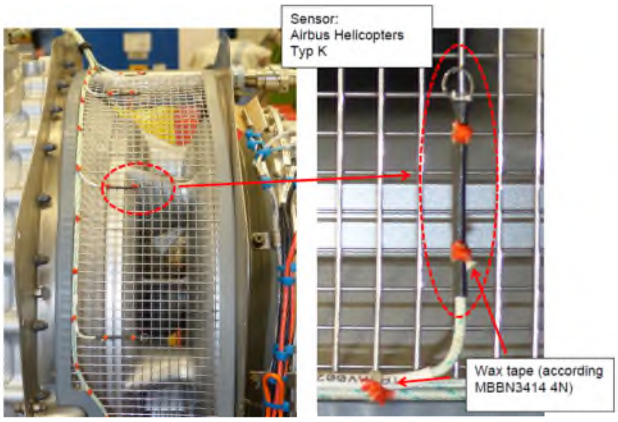

Figure 27: Inlet thermocouples installed on the engine FOD grid.

5.3. Flight test analysis method

The method for establishing the engine installed power classically employed in AHD is based on a comparative difference of normalized measured power between test bench and flight test data of the engines. It consists in opportunely normalizing the engine data recorded both in flight and on the test-cell allowing the direct comparison of tests made at different atmospheric conditions. Then, the difference between the power measured on the bench and that measured in flight (expressed either directly in normalized power or as percentage of the uninstalled power) provides a definition of installation loss (ΔPWSD, see an application example in *Figure 28*). The power difference can be built either at constant MGT or at constant NG. Being the PW206 governed by an MGT based control system, the difference between uninstalled and installed power is carried out at constant MGT.

A similar approach can be followed for the fuel flow, so as to establish a fuel flow increase with respect to the uninstalled engine. In this case, the difference between uninstalled and installed fuel flows is carried out at constant power (ΔWF, see an application example in *Figure 29*).

Being based on global performance measurements, the method accounts intrinsically for all installation loss components, including:

- inlet pressure losses;
- exhaust (incl. ejector) losses;
- losses due to the temperature increase in the helicopter air intake/duct;
- power extraction from the generator;
- inlet pressure and temperature distortions;
- Inlet swirl;
- miscellaneous losses (influence of engine compartment temperatures, oil temperature, etc.).

The parameters correction is based on the normalization formulas given in equation (10) for the corrected power, equation (11) for the corrected fuel flow, equation (12) for the corrected measured gas temperature and equation (13) for the corrected gas generator speed.

(8) $$\delta = \frac{PAMB}{PAMB(SL,ISA)} = \frac{PAMB}{101325\ Pa}$$

(9) $$\theta = \frac{OAT+273.15\ K}{OAT(SL,ISA)} = \frac{OAT+273.15\ K}{288.15\ K}$$

(10) $$PWSD_c = \frac{PWSD}{\delta^{XP}\theta^{YP}}$$

(11) $$WF_c = \frac{WF}{\delta^{XF}\theta^{YF}}$$

(12) $$MGT_c = \frac{MGT+273.15\ K}{\delta^{XT}\theta^{YT}} - 273.15\ K$$

(13) $$NG_c = \frac{NG}{\delta^{XN}\theta^{YN}}$$

Classically, the exponents in the correction formulas are derived from similarity analysis and are the following (Ref. 19):

- XP=XF=YT=1
- YP=YF=YN=0.5
- XT=XN=0

Specifically for the two engines equipping the Bluecopter demonstrator, optimal exponents fitting the measured engine characteristics have been provided by PWC.

The normalization method implicitly assume a constant NPT speed. This is not the case for the Bluecopter demonstrator engines, which operated on a wide NPT range.

Corrections accounting for the NPT variation were established by means of the EEPP.

The EEPP engine running lines ($PWSD_c$ vs. MGT_c and WF_c vs. $PWSD_c$), which are representative of a worst new production engine, were also employed to interpolate/extrapolate the reference Bluecopter engine data measured on the test cell (i.e. to generate the engine polar spline of bench test data in *Figure 28* and *Figure 29*).

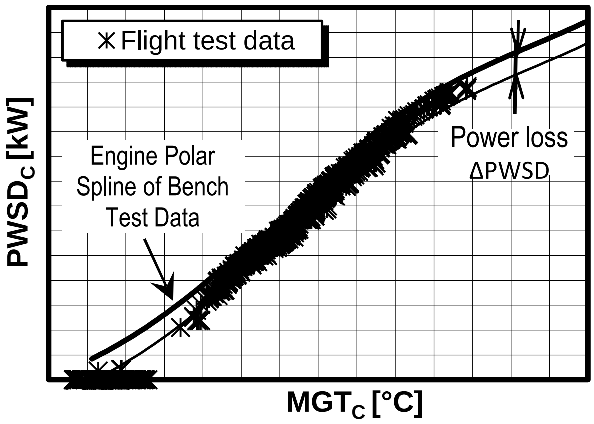

Figure 28: example of application of the normalization method for determining engine installation losses at constant MGT from flight test data.

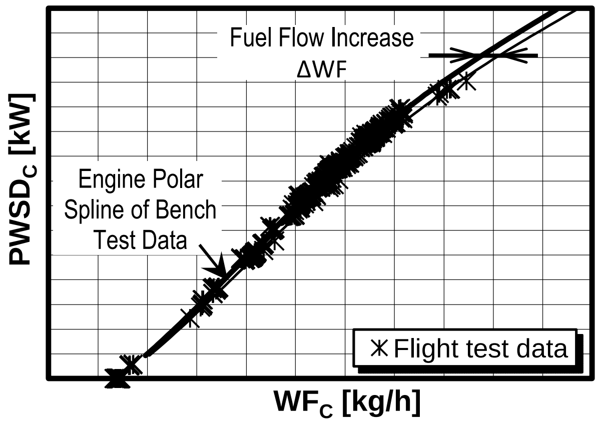

Figure 29: Example of application of the normalization method for determining engine fuel flow increase at constant power from flight test data.

Pressure sensors in the plenum chamber (*Figure 26*) have been taken to build an arithmetic average pressure, which should give a reasonable idea of the under-pressure to be found within the plenum. With it, a pressure loss parameter can be defined as in equation (14):

(14) $$\Delta P_{NORM} = \frac{\sum_{i=1}^{12} P_i/12}{PAMB}\frac{1}{\Delta P_{REF}}$$

This does not provide a quantitative and reliable measure of the inlet ram efficiency, however it can be applied to get a feeling about the pressure recovery induced by the scoop intake with respect to the ramp and check whether results of the engine performance analysis are consistent with the pressure measurements.

5.4. Summary of flight test results

For the benefit of synthesis, flight test results are presented here for the right hand side engine only. Qualitatively, the same conclusions can be drown from the analysis of the left hand side engine.

Figure 30 and *Figure 31* show the comparison between the static intake (conf. A) and ramp intake (conf. B) in terms of power loss and fuel flow increase respectively. Data are presented as function of true air speed and encompass hover to fast forward flight conditions. Looking at the engine power losses (*Figure 30*), the static and ramp intakes show similar results from low speed down to hover, where the differences between the two configurations lay within the measurement's scatter. Above ~60 kt, the advantage of the ramp intake becomes apparent. The relative difference in power loss is 2% to the advantage of the ramp intake, with nearly constant offset above approximatively 80 kt. The benefits in terms of fuel consumptions are less evident (*Figure 31*): below 60 kt, the static intake has a slightly lower fuel flow, whereas only at the highest speeds, approximately between 140 and 150 kt, the ramp intake does show a fuel consumption reduction of about 0.5%. These results are globally in line with the numerical predictions discussed in chapter 3.5 (Table 2 and Table 3).

Figure 32 and *Figure 33* show the same comparison between the ramp intake (conf. C) and scoop intake (conf. D). In terms of power loss at constant MGT (*Figure 32*), the two configurations show similar results at low speed, up to about 60 kt. For higher speeds, the scoop intake demonstrates significant gains, as expected. The maximum gain is approximatively 5% for speeds between 150 and 160 kt. The fuel flow rate reduction starts to be significant above 120 kt, with a maximum gain of approximatively 1.5% at 150 kt. These gains were somewhat under-predicted by the numerical analysis of chapter 3.5: the discrepancy may be partially due to the missing effect of total pressure distortion on the power and fuel flow predictions estimated through the EEPP, as explained in chapter 3.3. Total pressure distortion may have a significant effect on the performance of small turboshaft engines as experimentally and numerically investigated in Ref. 15.

While comparing the ramp with the scoop intake, it is interesting to assess the plenum under-pressure as expressed by equation (14). *Figure 34* shows the ΔP_{NORM} measured during ground runs with helicopter tight on ground. This kind of tests allow to increase the engine torque to higher levels, compatible to TOP or OEI conditions, which could not be tested in hover flight. Despite the flight test data reported in *Figure 32* show limited difference between ramp and scoop in hover flight, the faster growth of ΔP_{NORM} against engine torque, which characterizes the scoop intake, implies that higher power losses in hover are to be expected for the scoop intake when the power demand increases. The power loss increase due to this effect is estimated to be of about 1%. *Figure 35* shows the ΔP_{NORM} evolution against the true air speed in forward flight. The measurements for the scoop intake highlight a decreasing static pressure drop in the plenum chamber, with negative plenum under-pressure for speeds above 90 kt, indicating efficient ram compression. The static pressure drop instead increases with speed for the ramp intake.

Finally, the potential aerodynamic drag increase introduced by the scoop intake was analyzed by comparatively assessing the total helicopter power required in fast level flight for configurations C and D. Indeed, an increase of aircraft drag, due to the introduction of the scoop intake, would be visible in terms of parasite power, which increases with the true air speed to the power of three. Unfortunately, due to the different phases of the flight test campaign in which configurations C and D flew, a back-to-back comparison of the helicopter total power required with similar flight conditions was not possible. Both the ramp and scoop intake flew at the same pressure altitude (5000 ft), but with different OAT and different GM (350 kg higher gross mass for the scoop intake). The higher gross mass and different atmospheric conditions result in higher power required for configuration D (scoop intake), so as the two flights cannot be compared directly. In order to overcome this drawback, the two flight tests have been recomputed with the Bluecopter Demonstrator performance estimation model implemented in GENSIM. The performance model is representative of configuration C (GRC1 main rotor and ramp intake) in terms of aeromechanic characteristics and drag. *Figure 36* shows the GENSIM power required calculations for the test conditions recorded for configuration C (ramp) and D (scoop) respectively, superimposed to the corresponding test results.

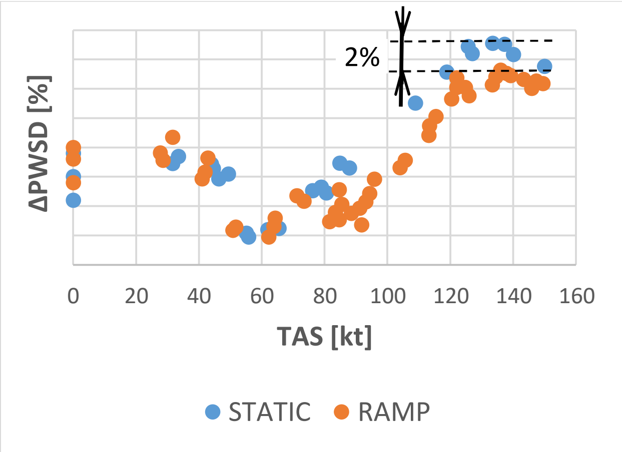

Figure 30: Comparison between static intake (Conf. A) and ramp intake (Conf. B) engine power loss at constant MGT in level flight.

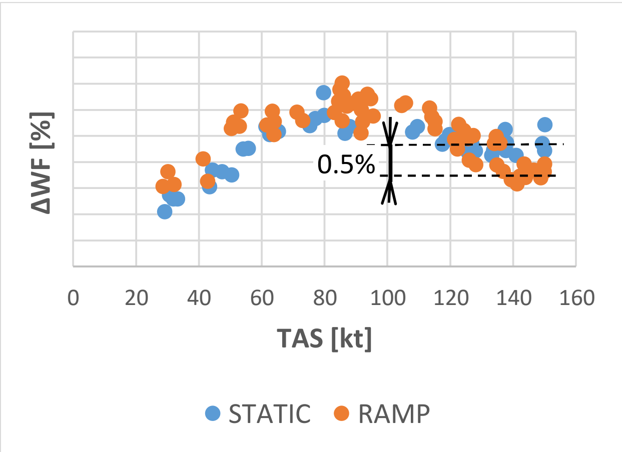

Figure 31: Comparison between static intake (Conf. A) and ramp intake (Conf. B) engine fuel flow loss at constant power in level flight.

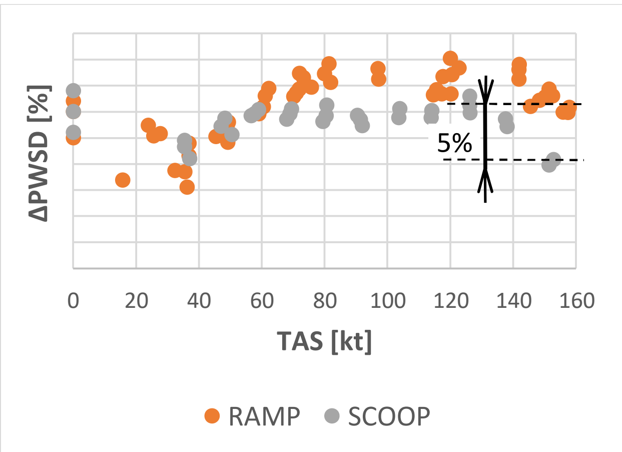

Figure 32: Comparison between ramp intake (Conf. C) and scoop intake (Conf. D) engine power loss at constant MGT in level flight.

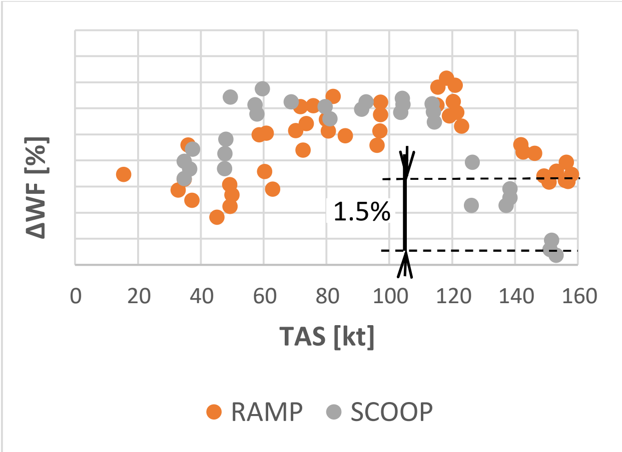

Figure 33: Comparison between ramp intake (Conf. C) and scoop intake (Conf. D) engine fuel flow loss at constant power in level flight.

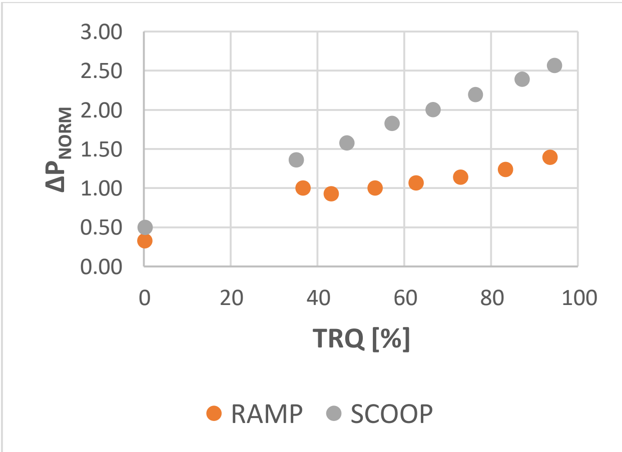

Figure 34: Comparison between ramp intake (Conf. C) and scoop intake (Conf. D) pressure loss vs. engine torque during ground run.

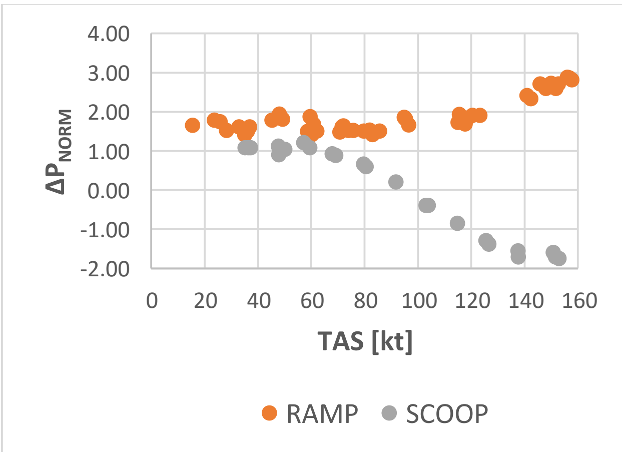

Figure 35: Comparison between ramp intake (Conf. C) and scoop intake (Conf. D) pressure loss vs. air speed in level flight.

The power required diagrams show that the GENSIM model is able to match the helicopter power demand, in both flight cases, without any need of increasing the fuselage drag on configuration D. In agreement with the numerical analysis of chapter 3.5, it can be concluded that the scoop intake is drag-neutral in comparison to the ramp intake.

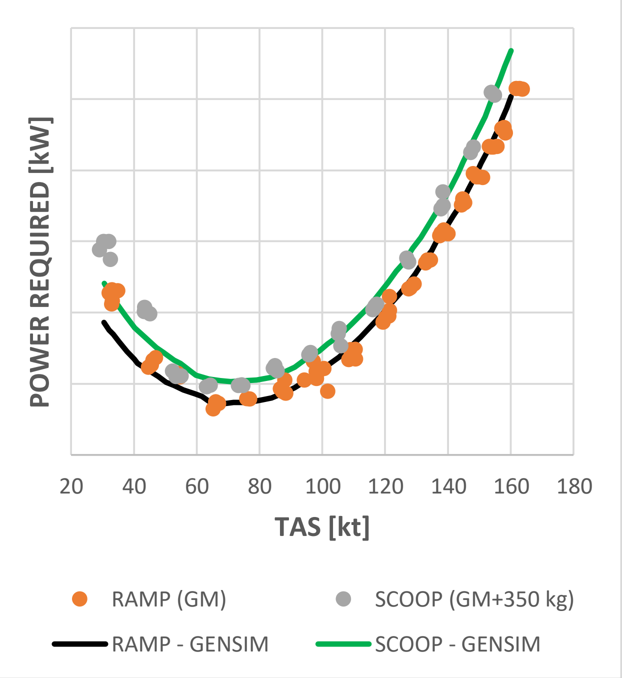

Figure 36: Comparison between ramp intake and scoop intake power required in level flight, drag estimation.

6. CONCLUDING REMARKS

The main activities carried out in the frame of the Bluecopter demonstrator engine air intake development have been presented. Focus of the studies was the air intake aerodynamic efficiency whose improvement consequently led to enhanced engine performance (higher power available and lower fuel consumption). Activities were grouped in three main development steps, namely the initial intake development and design optimization supported by numerical tools, wind tunnel testing and final flight test verification. The main results of the three phases are discussed throughout the paper.

The main conclusions can be summarized as follows:

1. Numerical analysis, wind tunnel measurements and flight tests all returned consistent results in terms of configuration ranking and magnitude of the possible aerodynamic and engine performance benefits;
2. The static intake, most common choice on small helicopters due to its simple, low weight architecture, guarantees best engine performance at low speed down to hover;
3. However, it is possible to optimize a static intake architecture with slight modifications on the cowling, without any weight penalty, by implementing a ramp, and by slightly modifying the plenum chamber, in order to gain interesting improvements in fast level flight conditions. For the specific case of the Bluecopter demonstrator equipped with the optimized ramp intake, up to 2% engine power increase at constant MGT and -0.5% fuel flow reduction at constant power could be demonstrated in flight, with respect to the static intake;
4. The aerodynamic efficiency of a static intake architecture can be further optimized by the introduction of retrofit solutions such as inlet guide vanes and rear spoilers, as demonstrated by wind tunnel measurements (Ref. 9);
5. To further improve engine performance in level flight, a scoop intake architecture can be considered. Through appropriate design choices, especially concerning the scoop capture area, it is feasible to realize a scoop intake with only moderate engine performance penalties at low speed with respect to a static intake, and neutral in terms of drag. For the specific case of the Bluecopter demonstrator equipped with the optimized scoop intake, up to 5% engine power increase at constant MGT and -1.5% fuel flow reduction at constant power could be demonstrated in flight, with respect to the ramp intake. The power available loss at low speed is estimated to be approximatively 1% whereas the drag increase is zero.

Author contact:

Andrea Garavello: andrea.garavello@airbus.com
Thomas Kneisch: thomas.kneisch@airbus.com
Markus Müller: markus.mueller3@airbus.com
Alessandro D'Alascio: alessandro.dalascio@airbus.com

7. ACKNOWLEDGMENTS

The development of the Bluecopter™ demonstrator technologies was partially funded by the European Community's Seventh Framework Program (FP/2007-2013) for the Clean Sky Joint Technology Initiative and by the German Luftfahrtforschungsprogramm (LuFo) IV.

8. REFERENCES

1. M. Bebesel, A. D'Alascio, S. Schneider, S. Guenther, F. Vogel, C. Wehle, D. Schimke, "*Bluecopter demonstrator – an approach to eco-efficient helicopter design*", Airbus Helicopters Deutschland GmbH, Germany, proceedings of 41st European Rotorcraft Forum 2015;

2. A. Kus, S. Schneider, M. Hollands, R. Rammer, O. Dieterich, M. Priems, "*GRC1: An Advanced Five-Bladed Bearingless Main Rotor Dynamics and Acoustics from Draft to Flight Test*", Airbus Helicopters Deutschland GmbH, Germany, proceedings of the AHS International 74th Annual Forum & Technology Display, Phoenix, Arizona, USA, May 14-17, 2018;

3. A. D'Alascio, S. Mores, F. Le Chuiton, M. Bebesel, Q. Zhang, "*Aerodynamic blunt aft body*", Airbus Helicopters Deutschland GmbH, patent EP12400029.0A;

4. S. Schneider, R. Heger, P. Konstanzer, "*Bluecopter demonstrator – state of the art in low noise design*", Airbus Helicopters Deutschland GmbH, Germany, proceedings of 42nd European Rotorcraft Forum 2016;

5. R. Rammer, A. Kus, J.B. Maurice, O. Dieterich, P. Konstanzer, "*Bluecopter demonstrator – mastering dynamic challenges*", Airbus Helicopters Deutschland GmbH, Germany, proceedings of 42nd European Rotorcraft Forum 2016;

6. F. Knoth, "*Aerodynamic Analyses of Novel Helicopter Engine Air Intakes*", PhD dissertation, 2020, Institute of Aerodynamics and Fluid Mechanics of the Technische Universität München; https://mediatum.ub.tum.de/1484576

7. F. Knoth, J.H. You, C. Breitsamter, "*Aerodynamic analysis of helicopter side intake variants by full scale wind tunnel measurements*", proceedings of 41st European Rotorcraft Forum 2015;

8. F. Knoth, C. Breitsamter, "*Aerodynamic Testing of Helicopter Side Intake Retrofit Modifications*", Aerospace 2017, 4(3), 33; https://doi.org/10.3390/aerospace4030033 https://www.mdpi.com/2226-4310/4/3/33

9. F. Knoth, C. Breitsamter, "*Aerodynamic testing of helicopter novel air intakes*", In Proceedings of the 30th Congress of the International Council of the Aeronautical Sciences, Daejon, Korea, 25–30 September 2016; pp. 1–13.

10. F. Knoth, C. Breitsamter, "*Numerical and Experimental Investigation of Helicopter Engine Air Intakes*". Deutscher Luft- und Raumfahrtkongress [DGLRK2015-0215], 2015, pp. 1-10

11. Pratt & Whitney Canada. Cross-section picture PW206B2. www.pwc.ca/en/engines/pw200. Accessed on 27 November 2017;

12. Ansys Fluent User manual, 2010 release 13; Chapter 7.3.19, Porous jump boundary conditions.

13. S. F. Hoerner NY, "*Fluid-Dynamic Drag*", Published by the Author, 1965, 3-24

14. W. Johnson, "*A History of Rotorcraft Comprehensive Analyses*", Proceedings of the American Helicopter Society 69th Annual Forum, May 2013.

15. F. Fuchs, V. Gümmer, „*Helicopter engine simulations accounting for intake distortion*", Lehrstuhl für Turbomaschinen und Flugantriebe, Technische Universität München, Deutscher Luft- und Raumfahrtkongress 2020 Document ID: 530046.

16. E.L. Goldsmith, J. Seddon, "*Intake Aerodynamics*", Collins Professional and Technical Books, 1985.

17. T. Breuer, N. C. Bissinger, "*Basic Principles–Gas Turbine Compatibility–Intake Aerodynamic Aspects*", Encyclopedia of Aerospace Engineering.: John Wiley & Sons, 2010, EAE487.

18. A. Vuillet, "*Aerodynamic design of engine air intakes for improved performance*", Societe Nationale Industrielle Aerospatiale, Helicopter Division, Marignane, France, proceedings of 6th European Rotorcraft Forum 1980;

19. P.P. Walsh, P. Fletcher, "*Gas Turbine Performance*", second edition, Blackwell Science, 2004.